Korean J. Chem. Eng., 39(11), 2991-3002 (2022)
DOI: 10.1007/s11814-022-1271-4

pISSN: 0256-1115
eISSN: 1975-7220

Flow behavior of gadolinium doped ceria under different polymeric and hydrodynamic environment for tape casting application

Lakshya Mathur*, Hohan Bae*, Yeon Namgung*, Jun-Young Park,†, and Sun-Ju Song*,†**

*Department of Materials Science and Engineering, Chonnam National University, Gwangju 61186, Korea
**HMC, Department of Nanotechnology and Advanced Materials Engineering, Sejong University, Seoul 05006, Korea
(*Received 10 May 2022 • Revised 25 July 2022 • Accepted 21 August 2022*)

Abstract−The present investigation consists of a comprehensive analysis of the rheological properties of tape casting slurry and optimization of its composition through rheological results. Formulation of slurry consists of gadolinium doped ceria (GDC) powder, solvent (ethanol and toluene), dispersant (menhaden fish oil), plasticizer (benzyl butyl phthalate160 and polyethylene glycol 8000), and binder (polyvinyl butyral 98). The slurry exhibits pseudoplastic behavior, which is drastically affected by a minute change in powder content. These changes in the flow properties were traced in terms of shear dependence (m) and fractal dimension (d_f) of aggregates, along with the trend of growth in aggregate size (R) and its volume fraction (ϕ_a) in the presence of different additives. These results suggest that the GDC particles tend to form large, rigid aggregates, which show appearance of yield stress even at ϕ>0.06. Furthermore, the addition of polymeric chains in the form of additives causes the steric stabilization of aggregates and formation of their 3-D network structure, which suppresses the sedimentation velocity to zero and provides crack-free and homogeneous green tape.

Keywords: Gelation Point, Shear Dependence, Fractal Aggregate Size, Solid Oxide Fuel Cell

INTRODUCTION

Gadolinium doped ceria (GDC) is a well-recognized electrolyte material due to its high oxygen ion conductivity, which makes it a suitable candidate as an electrolyte material in various electrochemical applications, such as solid oxide fuel cells (SOFCs), catalyst, gas sensing, and gas reforming [1-6]. In all these applications, the ionic conduction depends upon ohmic polarization, which wholly depends upon electrolyte thickness. Thus, it is vital to formulate dense, thin, and homogeneous electrolytes [7,8]. Among various formulation techniques, tape casting was found suitable for scalable fabrication of homogeneous electrolytes with well-controlled thickness, i.e., from 10 μm to 1 mm [9].

Dense electrolyte fabrication by tape casting essentially needs homogeneous and crack-free green tape along with some other properties, such as (i) defect-free green tape, (ii) good mechanical strength for handling, (iii) no peel off during casting, (iv) shape retention after casting. These properties depend upon rheological behavior and microstructure of suspension. The microstructure of a suspension deals with distribution of particles in the suspending medium, which is affected by the inter-particle potential and gap between them. In the case of attractive inter-particle potential and the short distance between them at higher solute content, the inter-particle collision results in aggregation [10]. This particle aggregation influences the rheological behavior of suspension. The key parameters that are responsible for the abrupt changes in suspension's rheological behavior, include solid particle loading (ϕ), shear rate (D), aggregate size (R), volume fraction of aggregate (ϕ_a), relative sedimentation velocity (U), percolation or gelation point (ϕ_g), shear dependence (m) and fractal dimension of aggregate (d_f). The gelation or percolation point denotes the volume fraction of the solid, beyond which the microstructure of suspension starts forming a network structure of aggregates [11]. All these parameters can be altered by the addition of additives such as dispersant, plasticizer, and binder in the suspension. Mostly, these polymeric additives create steric and electro-steric stabilization for aggregates and result in a stable suspension. Water, ethanol, toluene, butyl acetate, and their mixtures are generally used as a solvent [12-16]. Generally, the preference for dispersant lies among fish oil, polyvinyl pyrrolidone (PVP), polyacrylic acid (PAA), ammonium polyacrylate (NH_4PAA), and sorbitan monooleate (Span 80) [14,17-20]. The commonly used plasticizers are glycerol, polyethylene glycol (PEG), polypropylene glycol (PPG), dibutyl phthalate (DBP), and benzyl butyl phthalate (BBP) [16-18,21-23]. In the case of binder, two major groups have been used for tape casting: cellulose ethers and vinyl or acrylic type polymer. Polyvinyl alcohol (PVA), polyvinyl butyral (PVB), polyvinyl acetate (PVAc), polyvinyl pyrrolidine (PVP), polyacrylic acid (PAA), poly ethyl acrylate (PEA), poly methacrylic acid (PMAA), polymethyl methacrylate (PMMA) are some commonly used binders [14,21-24]. All of these additives synergistically affect the flow behavior of the slurry. Such as addition of dispersant and plasticizer to the solvent decrease the viscosity of the slurry by steric stabilization and extend the $Ø_g$. This extension allows the dissolution of a higher amount of solid particles in the solvent without creating a saturated environment where the 3-D structure of aggregates formed; this results in a high yield of final tape. Along with this assistance,

†To whom correspondence should be addressed.
E-mail: jyoung@sejong.ac.kr, song@chonnam.ac.kr

the presence of plasticizer also increases the plasticity of the green tape by breaking the close alignment and bonding of other polymeric additives under hydrodynamic conditions [25,26]. The addition of binder enhances the reversible pseudoplastic behavior of the suspension so that it can hinder the cracking of green tape at the time of shear application by the restoration of microstructure. However, this phenomenon also depends upon the total volume of solid loading [27].

The greater the amount of solid powder, the greater the final yield. Highly dense microstructure is an essential condition for solid electrolyte application. However, addition of additives in tape casting to achieve homogeneous crack free green tape reduces the density of sintered tape. In this context, different researchers found some combination of solute particles and additives to get a dense, homogeneous tape with the highest yield. Luo et al. [28] formulated 51.5% dense GDC powder's tape with 55 vol% of solid loading with water as a solvent. Due to the water-based system, a separate surfactant was also used to reduce the surface tension and enhance the wettability at the time of casting [29]. Meier et al. [30] also formulated GDC based tape with organic solvent (butyl acetate). Low surface tension and good wettability of butyl acetate eliminates the use of surfactant and leads to the formation of a 92% dense film with 42 vol% GDC loading. Henceforth, to eliminate the use of surfactants, the use of a polar solvent is recommended. Wang and Gao [27] examined the electro-kinetic properties of Y-TZP suspensions for different polyelectrolyte dispersants. They found that the addition of dispersant allows them to enhance Ø for high yield. Till 30 vol% solid loading, Newtonian behavior was observed which transformed to pseudoplastic at 47 vol%. This behavior indicates that until the stabilization effect dominates, the flow behavior will remain Newtonian.

The present work analyzed the effect of different hydrodynamic conditions on the aggregation process of GDC solute particles for the tape casting application. In this order, the viscosity as function

Table 1. Slurry formulation of GDC for flow behavior analysis

Sections	Powder	Solvent		Dispersant	Plasticizer		Binder
	GDC (volume fraction) (Ø)	Ethanol (volume fraction)	Toluene (volume fraction)	Fish oil (volume fraction)	PEG-8000 (volume fraction)	BBPS-160 (volume fraction)	PVB-98 (volume fraction)
Segment-I (S-I)	0.02	0.5130	04669	-	-	-	-
	0.04	0.5026	0.4573	-	-	-	-
	0.06	0.4921	0.4478	-	-	-	-
	0.08	0.4816	0.4383	-	-	-	-
	0.10	0.4712	0.4287	-	-	-	-
	0.12	0.4607	0.4192	-	-	-	-
	0.14	0.4502	0.4097	-	-	-	-
Segment-II (S-II)	0.02	0.5015	0.4564	0.022	-	-	-
	0.04	0.4911	0.4468	0.022	-	-	-
	0.06	0.4806	0.4373	0.022	-	-	-
	0.08	0.4701	0.4278	0.022	-	-	-
	0.10	0.4596	0.4183	0.022	-	-	-
	0.12	0.4492	0.4087	0.022	-	-	-
	0.14	0.4387	0.3992	0.022	-	-	-
Segment-III (S-III)	0.02	0.4701	0.4278	0.022	0.05	0.01	-
	0.04	0.4596	0.4183	0.022	0.05	0.01	-
	0.06	0.4492	0.4087	0.022	0.05	0.01	-
	0.08	0.4387	0.3992	0.022	0.05	0.01	-
	0.10	0.4282	0.3897	0.022	0.05	0.01	-
	0.12	0.4178	0.3801	0.022	0.05	0.01	-
	0.14	0.4073	0.3706	0.022	0.05	0.01	-
Segment-IV (S-IV)	0.02	0.4282	0.3897	0.022	0.05	0.01	0.08
	0.04	0.4178	0.3801	0.022	0.05	0.01	0.08
	0.06	0.4073	0.3706	0.022	0.05	0.01	0.08
	0.08	0.3968	0.3611	0.022	0.05	0.01	0.08
	0.10	0.3863	0.3516	0.022	0.05	0.01	0.08
	0.12	0.3759	0.3420	0.022	0.05	0.01	0.08
	0.14	0.3654	0.3325	0.022	0.05	0.01	0.08

of shear rate and sedimentation velocity of suspensions with various organic additives and GDC particles were measured. After analyzing these results based on some pre-existing equations and scaling relations, it was found that GDC particles tend to form rigid aggregates which are covered by long polymeric chains in order to obtain stabilized suspension for tape casting.

EXPERIMENTAL

1. Materials

Commercially available tape casting grade Gd^{3+} doped ceria (GDC) powder (Fuel cell materials) with surface area of 6.2024 $m^2 g^{-1}$ (shown in Fig. S1(b)) was used for slurry formulation along with ethanol (Daejung chemicals, Korea, 94.5% purity) and toluene (Junsei chemicals, Korea, 99.5% purity) as suspending medium. The scanning electron micrograph of commercial powder is shown in Fig. S1(c). Menhaden fish oil (Sigma Aldrich, analytical grade) and polyvinyl butyral 98 (PVB98) (molecular weight 40,000-70,000 g/mol) were used as dispersant and binder, respectively. Benzyl butyl phthalate160 (BBP160) (Victorchem Co. Ltd., Korea, molecular weight 312.37 g/mol) and polyethylene glycol 8000 (PEG8000) (Fisher scientific, molecular weight 400 g/mol) were used as the plasticizer.

2. Slurry Preparation for Rheological Measurement

The slurry for rheological analysis of GDC powder was prepared in different segments. For each segment (S-I-IV), the volume fraction of GDC powder was varied from 0.02-0.14. In each segment, a new additive was introduced and analyzed in terms of its viscosity and relative sedimentation velocity. The selection of additive and their amount was made according to Table 1. For slurry preparation in each segment, respective ingredients were mixed and ball-milled in the presence of zirconia balls where the weight ratio of GDC powder to zirconia balls was maintained constant 1 : 1. Ball milling was conducted in two-steps at a rotation speed of 80 rpm. In step I, GDC powder was dispersed in a mixture of ethanol and toluene in the presence of dispersant fish oil (if applicable). Furthermore, in step II, another ball milling of 24 hr was conducted in the presence of plasticizer and binder, whichever is applicable according to the segment. Henceforth, for segment S-I-II, the total ball milling is of 24 hr, whereas for segment S-III-IV, ball milling time increases to 48 hr.

3. Powder Characterization

The phase purity of commercial powder is shown in Fig. S1(a), which was examined by X-ray diffractometer (XRD) on D/MAX ultima III diffractometer (Rigaku, Japan) with an X-ray energy source of Cu Kα (λ=1.54056 Å). The surface and pore characteristics of the as-received GDC powder were investigated using an ASAP® 2020 Plus: Accelerated Surface Area and Porosimetry System (Micromeritics Instrument Corp., United States) and analyzed by Brunauer-Emmett-Teller (BET) method. The microstructure and morphology of the GDC powder were characterized using a field-emission scanning electron microscope (FE-SEM, Hitachi High-Tech S-4700, Japan) operated at an excitation voltage of 15 kV.

4. Rheological Measurement

Suspension prepared for the different segments was characterized in terms of viscosity and its derivative. A cone plate type viscometer (Model LVDV2T, Brookfield Co.) was used to measure the viscosity. The viscometer was implemented with spindle (CP-40 and CP-52) with a tilting angle of 4 degrees from the plate plane. Shear rate was varied in the range of 10 S^{-1} to 200 S^{-1} for all the measurements. The temperature was kept constant at 26 °C, by a continuous flow of water with heating and cooling unit. Each suspension was pre-sheared at 5 sec^{-1} for 30 sec, to avoid any thixotropic behavior.

The flow behavior of suspension was also examined in terms of its sedimentation velocity (U_P) with respect to the sedimentation velocity of the isolated dense particle (U_0). To examine the sedimentation behavior, a laboratory-made setup was used, which consisted of continuous water flow from water bath having heating and cooling unit, to maintain the temperature constant at 26 °C [31]. Furthermore, the suspension was kept in a measuring cylinder of 25 ml volume. The value of U_0 was calculated according to Stokes' law for the terminal velocity of the sphere falling in a fluid [32].

5. Tape Casting

The optimized ball-milled suspension was de-aired for 1 hr under vacuum conditions and cast on silicon-coated mylar film with the help of an 8-inch doctor blade [33]. The gap height of the casting blade was 1 mm, and the casting rate was maintained 5 mm/sec. After casting, the tape was left for 24 hr at 35 °C to get green strength, followed by pre-sintering at 1,000 °C for 2 h and sintering at 1,550 °C for 7 h in air. The schedule of pre-sintering also included the removal of organic additives at 400 °C for 1 hr. The ramp rate for pre sintering and sintering was maintained constant to 3 °C/min.

6. Theory and Models

To analyze the aggregate behavior under hydrodynamic conditions (such as m, d_f, R and ϕ_a), a number of theoretical models can be applied, such as Einstein's equation, Krieger-Dougherty (K-D) equation, and Casson's equation. Einstein provides a theoretical equation as an evidence of aggregation for particles in hydrodynamic conditions, as shown in Eq. (1). This relation is for hard spheres which are completely isolated from each other. The theoretical values of relative viscosity ($\eta_r = \eta/\eta_0$) extracted were compared with the experimental values and the difference between them reflects the aggregation. Herein, η_0 is the viscosity of suspending medium. Suspending medium used in this study is a mixture of ethanol and toluene which exhibits Newtonian flow under the shear rate of 10-200 sec^{-1}, with an average viscosity of 0.89 cP as shown in Fig. S1.

$$\frac{\eta}{\eta_0} = 1 + 2.5\phi \tag{1}$$

Krieger and Dougherty [34] proposed an equation to analyze the mechanism of the non-Newtonian flow of suspension of a rigid sphere, on the basis of concentration of solute. This equation is basically used for the evaluation of intrinsic viscosity as function of shear rate [10,31,32]. This relation between η_r and intrinsic viscosity ([η]) as a function of solid loading is shown in Eq. (2). Here ϕ_m, is the maximum particle volume fraction. We used ϕ_m=0.63 for random packing of hard sphere [32].

$$\frac{\eta}{\eta_0} = \left(1 - \frac{\emptyset}{\emptyset_m}\right)^{-[\eta]\emptyset_m} \tag{2}$$

However, when the solute's volume fraction is high enough, the interaction between them generates yield stress (τ_y) beyond ϕ_g. To

analyze the flow behavior of suspension in this regime, Casson [35] proposed an equation between τ_y and shear stress (τ), which is shown in Eq. (3). Herein, η_∞ and D shows the viscosity at infinite shear rate and shear rate, respectively.

$$\tau^{1/2} = \tau_y^{1/2} + (\eta_\infty \mathrm{D})^{1/2} \tag{3}$$

To further evaluate m and d_f for aggregate under hydrodynamic forces, relative sedimentation velocity of different suspensions was measured under gravity and the values were plotted against ϕ according to Eq. (4).

$$\frac{U_P}{U_0} \sim \emptyset^{\frac{(1-d_f)}{(3-d_f)}} \tag{4}$$

At low particle volume fraction, hydrodynamic clustering is negligible. If the spherical shape of particles and aggregates were assumed then, dependency of $[\eta]$ on ϕ_a and ϕ could be given according to Eq. (5). Here R and a are attributed to the radius of aggregate and particle, N is the number of particles in the aggregate [36]. Moreover, from mass-radius relation, N can be written in terms of R and a as shown in Eq. (6). The shear dependence of aggregates can be expressed as Eq. (8). From Eqs. (5)-(8), the relation between $[\eta]$ and D can be established according to Eq. (9). Here τ_b is attributed to bond strength between aggregates for inter-aggregate attraction [11].

$$[\eta] = 2.5\frac{\emptyset_a}{\phi} = 2.5\frac{1}{\mathrm{N}}\left(\frac{\mathrm{R}}{\mathrm{a}}\right)^3 \tag{5}$$

$$\mathrm{N} \propto \left(\frac{\mathrm{R}}{\mathrm{a}}\right)^{d_f} \tag{6}$$

$$\frac{\emptyset_a}{\phi} \propto \frac{1}{\phi_m}\left(\frac{\mathrm{R}}{\mathrm{a}}\right)^{3-d_f} \tag{7}$$

$$\frac{\mathrm{R}}{\mathrm{a}} \propto \left(\frac{\eta_0 \mathrm{D}}{\tau_b}\right)^{-m} \tag{8}$$

$$[\eta] \propto \left(\frac{\eta_0 \mathrm{D}}{\tau_b}\right)^{-m(3-d_f)} \tag{9}$$

Beyond $\emptyset_g$, the volume fraction of aggregate which consists of particles and suspending medium, tends to 1, and the $\eta_0 \mathrm{D} \sim \tau_y$. So the value of m and d_f in this regime can be extracted from Eq. (10) [32].

$$\tau_y \propto \tau_b \emptyset^{\frac{1}{m(3-d_f)}} \tag{10}$$

The parameters m and d_f are very useful for estimating the compactness, shape and shear dependence of aggregates [11]. Potanin [37] suggested that the interaction between particles for aggregation can be of two types: diffusion-limited cluster aggregation (DLCA) and reaction-limited cluster aggregation (RLCA). For the DLCA approach, the interaction between particles depends only upon inter-particle distance and the repulsive energy barrier between two approaching particles. If this repulsion barrier is much lower than the diffusive motion of particles, the aggregation will occur in more loose string-like shape and the aggregates will be termed as soft aggregates. For the RLCA approach, the interaction between particles depends upon angle between adjacent bonds and the repulsive energy barrier between two approaching particles. If this repulsion barrier is higher than the diffusive motion of particles, a closely packed aggregation will occur and the aggregates will be termed as rigid aggregates. DLCA aggregation process is very fast and the corresponding values of d_f and m lies between 1.7-1.9 and 0.4-0.5, respectively. However, the RLCA process is slower and the values of m and d_f lie between 0.2-0.4 and 2-2.2, respectively. Apparently, these values are wider than specified. To further estimate the changes in aggregate volume fraction (ϕ_a) as function of η_r, we can use the viscosity - concentration relation proposed by Quemada, as shown in Eq. (11) [38].

$$\frac{\eta}{\eta_0} = \left(1 - \frac{\emptyset_a}{\emptyset_m}\right)^{-2} \tag{11}$$

Based on the equations proposed by K-D, Casson and Quemada, some linear relations have been extracted to understand the behavior of R and ϕ_a as a function of ϕ, D and τ_y. These relations are shown in Eqs. (12)-(14).

$$\left[1 - (\eta_r)^{-\frac{1}{2}}\right] \propto \left(\frac{\phi}{\phi_m^2}\right)\left(\frac{\mathrm{R}}{\mathrm{a}}\right)^{3-d_f} \tag{12}$$

$$\frac{\mathrm{R}}{\mathrm{a}} \propto \left[\frac{\emptyset_m^2}{\emptyset}\left\{1 - (\eta_r)^{-\frac{1}{[\eta]\phi_m}}\right\}\right]^{\frac{1}{(3-d_f)}} \propto \left(\frac{\eta_0 \mathrm{D}}{\tau_b}\right)^{-m} \tag{13}$$

$$\left[1 - (\eta_r)^{-\frac{1}{[\eta]\phi_m}}\right] \propto \phi_a \left(\frac{\tau_y}{\tau_b}\right)^{m(3-d_f)} \tag{14}$$

Eqs. (5)-(9) and (12)-(14) show the dependency of aggregates' shape size and volume fraction on different parameters such as D, m and d_f. As can be seen from Eq. (6), if the fractal aggregate size is constant, the number of solute particles in aggregate is directly proportional to size of aggregate. However, considering the general values of d_f for soft and rigid aggregates 1.7-1.9 and 2-2.2, respectively, Eq. (6) suggests that the rigid aggregates consist of more solute particles than softer ones. Consequently, Eq. (7) implies that, the volume fraction for rigid aggregates is lower compared to soft aggregates. Moreover, after considering the general values of m for rigid and soft aggregate 0.2-0.4 and 0.4-0.5, respectively, Eqs. (8)-(9) demonstrate a clear picture of aggregate size. It implies that the rigid aggregates are bigger compared to soft aggregates. Conclusively, Eqs. (5)-(9) imply that rigid aggregates are bigger and consist of higher number of solute particles compared to softer aggregates. Based on these facts, some scaling relations were derived and shown in Eqs. (12)-(14). These equations show the tendency of aggregates under hydrodynamic conditions. Such as Eq. (12) supports that for a constant particle volume faction and d_f value the aggregate size is directly proportional to relative viscosity. This implies that bigger aggregates are difficult to break due to their rigidness. Similarly, Eq. (13) shows the relation of relative viscosity with shear rate as function of m. This implies that for a constant D value the softer aggregates show lower viscosity compared to rigid aggregates, which could be attributed to their loose string-like shape. It could also be attributed to the presence of fewer solute particles in the soft aggregate compared to rigid aggregate. Furthermore, Eq. (14) implies that for constant m and d_f value the higher viscosity of suspension

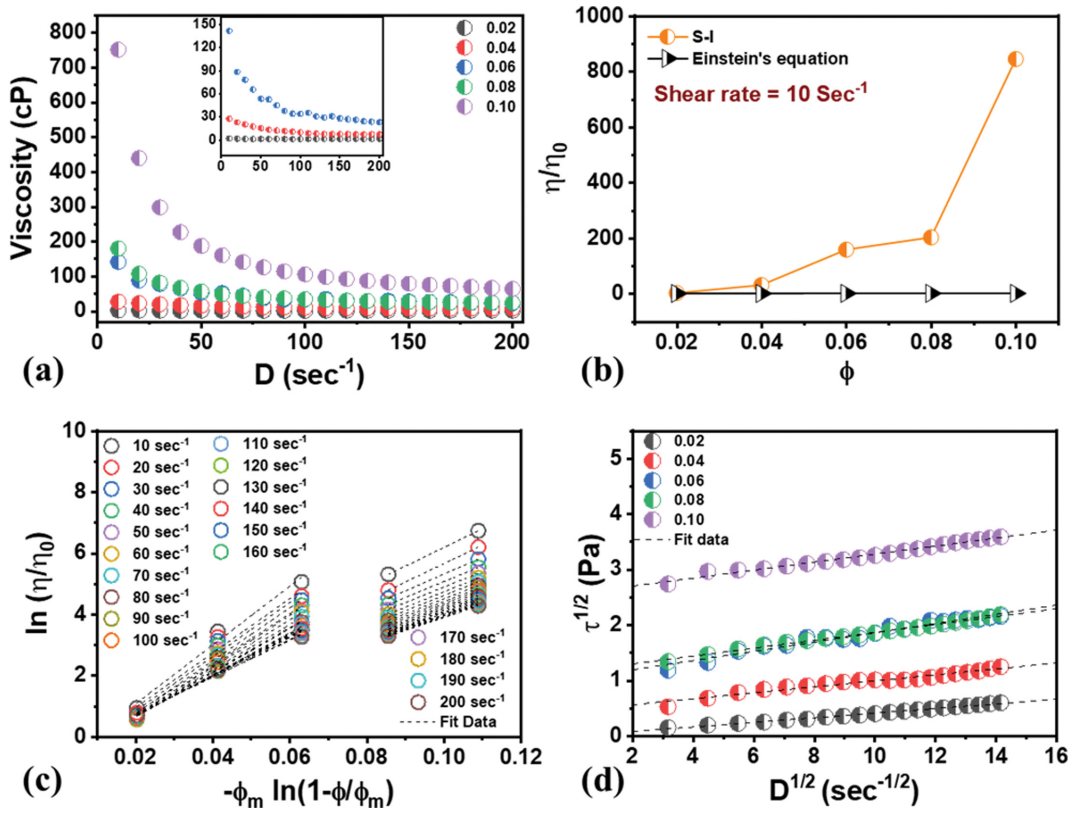

Fig. 1. (a) Variation of η as function of D, (b) η_r as function of ϕ, (c) Krieger-Dougherty plot, (d) Casson's plot, for S-I.

generates the yield stress.

RESULTS

1. Effect of Powder Concentration and Solvent

Segment-I (S-I) consists of the suspension of different volume fraction of GDC particles (0.02-0.10) in ethanol and toluene based suspending medium, as shown in Table 1. Fig. 1(a) demonstrates the variation of viscosity of these suspensions as a function of D. From this figure's inset, it can be observed that the flow behavior of suspension shows transition from Newtonian to non-Newtonian flow with increasing Ø from 0.02 to 0.04. For higher ϕ value the suspension shows shear thinning behavior at a low D value. To examine the hydrodynamic clustering of solute particles, the experimental value of η_r at D=10 sec^{-1} is plotted as a function of along with the theoretical value of η_r calculated according to Eq. (1). The higher experimental values indicate the initiation of aggregation of GDC particles from ϕ=0.04. This hydrodynamic clustering increases with the addition of solute particles. To estimate the ϕ_g of the suspension, the η_r at the different D value was plotted as a function of Ø according to Eq. (2) (K-D plot), as shown in Fig. 1(c). This plot exhibits a slope change at ϕ>0.04, which could be attributed to microstructural changes in the suspension beyond this point, as it could be the gelation point (ϕ_g=0.06) for this segment [31]. To analyze the variation of shear stress (τ) for different Ø value as function of D, Casson's plot was plotted according to Eq. (3) and demonstrated in Fig. 1(d). It can be observed from this figure that the τ increases with increasing Ø. The value of [η] was calculated from the slope of Fig. 1(c) for $\phi<\phi_g$ only, and plotted as a function of D in Fig. 2(b). Similarly, τ_y for different ϕ value was calculated from the intercept of Fig. 1(d) and plotted as a function of ϕ, in Fig. 2(c). This figure demonstrates that the τ_y for this segment appears significantly from ϕ>0.04, which supports ϕ_g=0.06. The relative sedimentation velocity of different suspensions in different segments was also examined under gravity as a function of ϕ, shown in Fig. 2(d). The relative sedimentation velocity for Segment-I decreases drastically with increasing ϕ and finally reaches zero at ϕ=0.12 and 0.14. This could be attributed to the increase in inter-aggregate attraction forces and the formation of a 3-D network of aggregates with increasing ϕ.

Fig. 1 demonstrates the different aspects of particle interaction and aggregate formation in Segment-I. The relation between η and D indicates that initially for ϕ=0.02, the solute particles are well separated and exhibit Newtonian flow behavior. However, increasing leads to inter-particle attraction and causes aggregation or hydrodynamic clustering and originates non-Newtonian flow behavior of the suspension. These aggregates were made up of solute particles and suspending medium, which causes two types of forces: hydrodynamic forces and inter-aggregate attraction forces. Here, the hydrodynamic force consists of both the force applied by the suspending medium present inside and outside the aggregate [39]. Viscosity of the suspension increases until the inter-aggregate attraction force is dominating. On applying shear stress, the hydrodynamic force dominates and the breakdown of aggregates occurs, which results in shear thinning [28]. On increasing the solute concentration, the inter-aggregate attraction forces dominate,

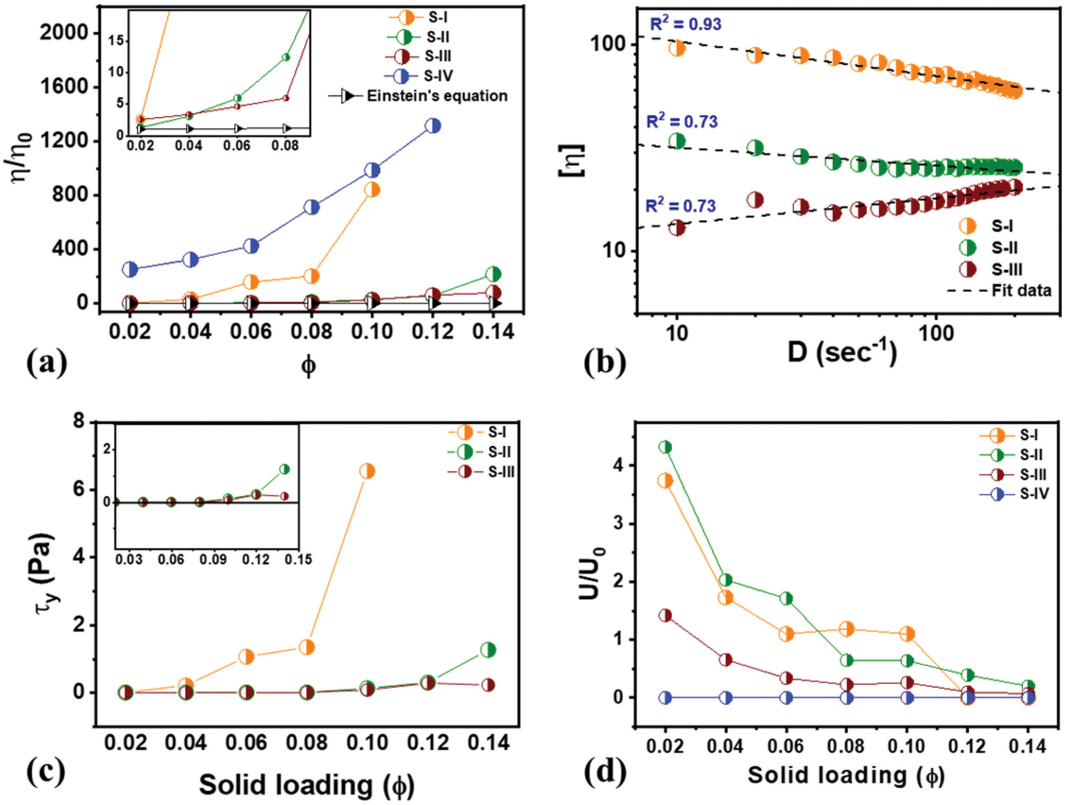

Fig. 2. Comparison of (a) η_r as function of ϕ, (b) $[\eta]$ as function of D, (c) variation of τ_y and (d) U as function of ϕ for S-I-IV.

which leads to microstructural changes in the suspension and causes highly aggregated slurry beyond ϕ_g. GDC particle aggregation starts from ϕ=0.04, as suggested by Fig. 1(b); however, it appears significantly after reaching ϕ=0.06. Similarly, the τ_y also appears significantly beyond ϕ=0.06, which supports ϕ_g=0.06. On further enhancement of solute concentration up to ϕ=0.10, inter-aggregate attraction force constructs a 3-D network of aggregates, which exhibit an abrupt increase in the η value to 751 cP at D=10 sec^{-1}. Beyond this point, the slurry's viscosity is higher than the capacity of the instrument and U becomes zero. The values of m and d_f were extracted from the slope of the logarithmic curve of Fig. 2(c) and (d), by employing Eqs. (4) and (10). The values obtained for m and d_f are 0.22 and 1.9, respectively. These values are close enough to the values for the reaction limited cluster aggregation (RLCA) approach, which is also supported by the linearity of Fig. 2(b) [31]. This implies that aggregates formed in this segment were rigid.

2. Effect of Powder Concentration in the Solvent-dispersant System

Segment-II (S-II) refers to the variation of ϕ in the solvent-dispersant system. The volume fraction of dispersant was kept constant at 0.022, and GDC powder volume fraction was varied from 0.02-0.14, as shown in Table 1. In the present work, fish oil was used as the dispersant, which is made up of a bulky organic group, omega-3 fatty acids ($C_{60}H_{92}O_6$). A tiny amount of this bulky group can cover a large concentration of solute particles. The variation of this suspension's viscosity as a function of D is shown in Fig. 3(a). From the inset of this figure, it can be observed that similar to S-I, the flow behavior of suspension in S-II transforms from Newtonian to non-Newtonian after Ø=0.02. This transition to non-Newtonian flow exhibits shear thinning at low D value followed by shear thickening at high D value up to ϕ=0.08. On further enhancement of ϕ, this shear thickening is suppressed and aggregation increases significantly, as shown in Fig. 3(a) and (b). To analyze the effect of this aggregation on the microstructure and to find the ϕ_g, a K-D plot was created according to Eq. (2), as shown in Fig. 3(c). Similar to the previous segment, this segment also exhibits a slope change at ϕ=0.10, which could be attributed to microstructure change due to high aggregation beyond this point, as it could be the gelation point (ϕ_g=0.10). To examine the variation of τ with ϕ, Casson's plot was constructed as shown in Fig. 3(d). This curve demonstrates that τ value increases with ϕ. The $[\eta]$ value was calculated from the slope of Fig. 3(c) for $\phi<\phi_g$ only, and plotted as a function of D in Fig. 2(b). Similarly, τ_y for different ϕ value was calculated from the intercept of Fig. 3(d) and plotted as a function of ϕ, in Fig. 2(c). This figure demonstrates that this segment τ_y appears significantly from ϕ>0.08, which supports ϕ_g=0.10. Relative sedimentation velocity for different solute concentration in this segment is shown in Fig. 2(d). S-II's relative sedimentation velocity has almost similar trends as S-I; however, fish oil's weight could be the possible reason behind its slightly high value compared to S-I.

The overall value of η in this segment is almost four times lower compared to S-I; this could be attributed to the steric stabilization of GDC particles by polymeric chains of fish oil [9]. This stabilization also affects the hydrodynamic clustering of solute particles in the suspension and causes shear thinning at low D value

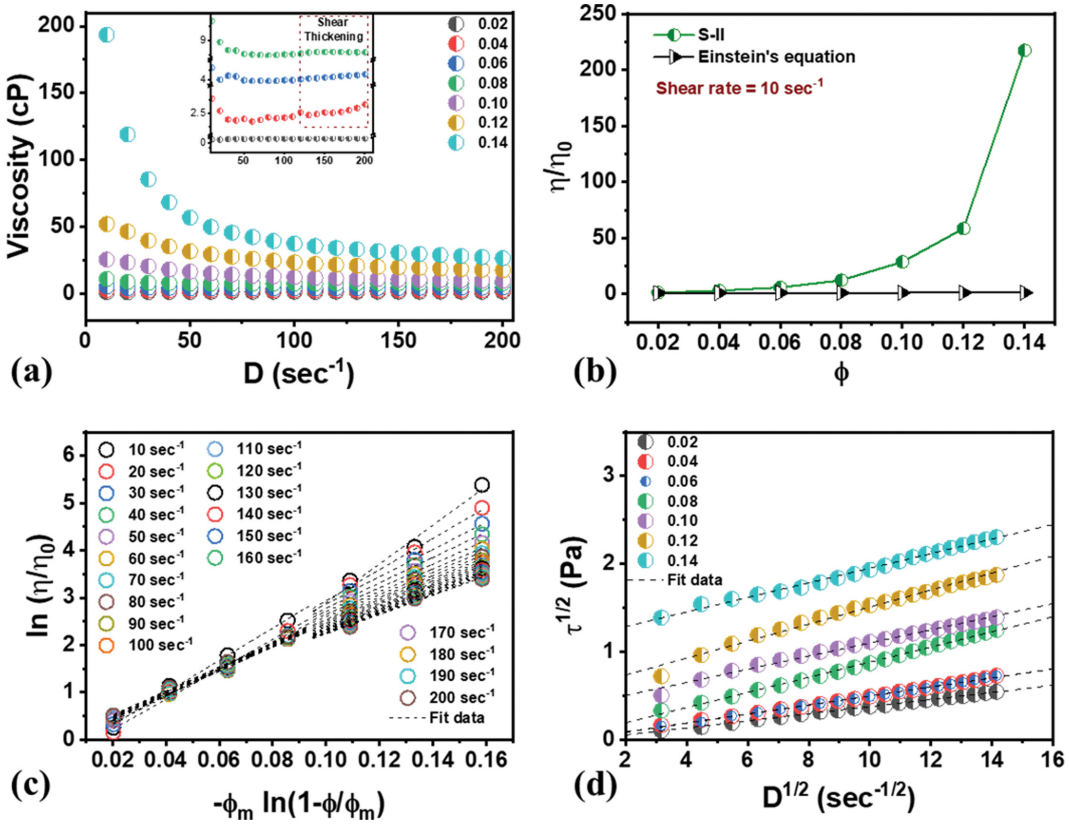

Fig. 3. (a) Variation of η as function of D, (b) η_r as function of ϕ, (c) Krieger-Dougherty plot, (d) Casson's plot, for S-II.

due to breaking of aggregates, followed by shear thickening at high D value for ϕ=0.04-0.08. This anomalous behavior of η (shear thickening) in this regime can be explained on the basis of forces acting on aggregates under the presence of fish oil. One of the forces represents the repulsion barrier caused by polymeric chains (steric stabilization), and the other is associated with the attractive van der Waal force. The repulsion barrier can only be reduced when the inter-aggregate distance is sufficiently low to overlap the surface layers, which could only be achieved either by increasing ϕ or by applying high shear forces. In both cases, flocculated aggregates tend to increase the viscosity very high. Galindo-Rosales [40] suggested that polar solvents are not good for dispersion of alkyl group (fish oil) containing polymers. This makes the steric interaction potential negative, which causes a net attractive interaction when adding it to the van der Waal forces. This favors the hydrodynamic clustering of polymer covered primary aggregates at high concentration or shear force [40,41]. In the present study, the polymeric chains cover the solute particles very well at low ϕ value and cause a high repulsion barrier. This barrier was reduced with the application of high shear rate, which caused the actuation of attractive steric forces and reduction between inter aggregate distance, which led to an increase in η with D (shear thickening). Moreover, for ϕ>0.08, the concentration of aggregates was high enough and positioned with a minimum inter-aggregate distance, which cannot be reduced by applying a high shear rate. This inability to minimize inter-aggregate distance suppresses the shear thickening behavior and causes microstructural changes in suspension for ϕ>0.08. This is also supported by the appearance of τ_y for ϕ>0.08, which confirms the ϕ_g=0.10. The value of m and d_f was extracted from the slope of the logarithmic curve of Fig. 2(c) and (d), by employing Eqs. (4) and (10). The values obtained for m and d_f are 0.29 and 2.19, respectively. These values are close enough to the values for RLCA approach, which implies that aggregates formed in this segment were also rigid [31]. The nonlinearity of Fig. 2(b) for S-II could be attributed to shear thickening at high D value for the regime $\phi<\phi_g$.

3. Effect of Powder Concentration in Solvent-dispersant-plasticizer System

Segment-III (S-III) refers to the variation of ϕ in a system having a combination of solvent, dispersant, and plasticizer. The plasticizer is a key parameter for the final tape's flexibility, which breaks the close bonding of other polymer's structure and creates new bonds with them. The efficiency of plasticizer is determined by the coefficient of interaction with other polymers [25,26]. A combination of polyethylene glycol (PEG) and benzyl butyl phthalate160 (BBP160) is an effective plasticizer, which can react with preadsorbed polymeric dispersant and soften the binder as well [42, 43]. The variation of η as a function of D in the range of 10 to 200 sec^{-1} is shown in Fig. 4(a). Compared to S-I and II, the overall value of η decreases drastically after the addition of plasticizer; however, transition from Newtonian to non-Newtonian flow remains the same at ϕ>0.02. The abrupt decrease in the suspension's viscosity in this segment could be attributed to the electro-steric stabilization of aggregates under the presence of polymeric chains of plasti-

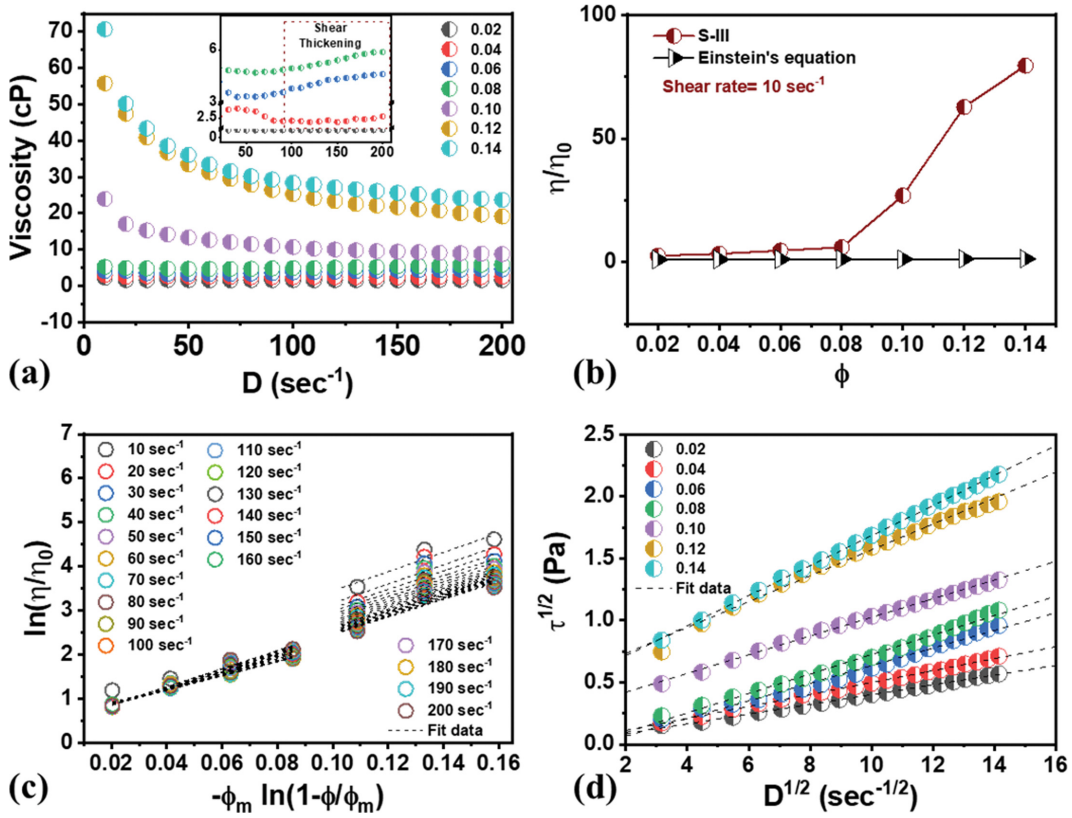

Fig. 4. (a) Variation of η as function of D, (b) η_r as function of ϕ, (c) Krieger-Dougherty plot, (d) Casson's plot, for S-III.

cizer [9]. As can be observed from the inset of Fig. 4(a), the addition of plasticizer does not disturb the shear thickening behavior at low ϕ (0.04-0.08) and its suppression at high ϕ value originated due to steric stabilization in S-II. The hydrodynamic clustering also decreases after adding plasticizers, as shown in Fig. 4(b). To analyze the effect of this aggregation on the microstructure and to find out the ϕ_g, K-D plot was created according to Eq. (2), as shown in Fig. 4(c). Similar to the previous segment, a slope change in this figure at ϕ=0.10 indicates its candidature for the ϕ_g. Moreover, Casson's plot for this Segment is shown in Fig. 4(d), demonstrating the increases in τ value with ϕ. The [η] value of the suspension was calculated from the slope of Fig. 4(c) for $\phi<\phi_g$ only, and plotted as a function of D in Fig. 2(b). Similarly, τ_y for different ϕ value was calculated from the intercept of Fig. 4(d) and plotted as a function of ϕ, in Fig. 2(c). This τ_y value appears significantly from ϕ>0.08, which supports ϕ_g=0.10. Relative sedimentation velocity for different ϕ value in this segment is shown in Fig. 2(d), which is almost two-times lower than previous segments. The U value decreases with ϕ and reaches almost zero at ϕ>0.10. The values of m and d_f extracted for this segment are 0.27 and 2.18, respectively, comparable to S-II. These values also imply that particle aggregation is reaction limited and rigid [31].

4. Effect of Powder Concentration in Solvent-dispersant-plasticizer-binder System

Segment-IV (S-IV) refers to the variation of ϕ in a system consisting of solvent, dispersant, plasticizer, and binder, as shown in Table 1. The key role of binder addition in any tape casting slurry

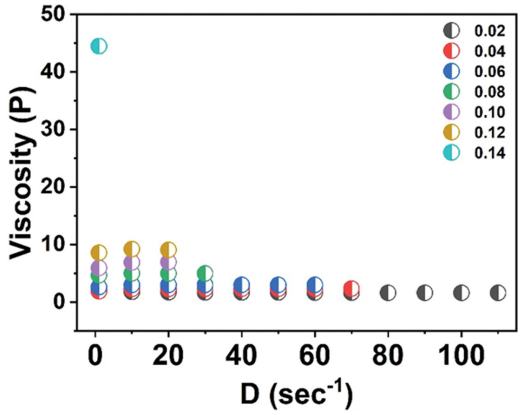

Fig. 5. Variation of η as function of D for S-IV.

is to provide green strength to the tape by making inter-particle bridges [26]. Polyvinyl butyral 98 was added as the binder in the suspension. Along with other additives, the volume fraction of binder was kept constant at 0.08 and ϕ was varied from 0.02-0.14. The variation of η with D and sedimentation behavior for different suspensions is shown in Fig. 5(a) and Fig. 2(d). It can be observed that the addition of binder eliminates the shear thinning behavior and shows Newtonian behavior in our desired range of D (1-110 sec^{-1}). Additionally, enhancement of ϕ in the system increases the η gradually, and for ϕ=0.14 viscosity enhanced exponentially. A cone plate type viscometer with CP-52Z spindle has

an upper limit of 9300/N for viscosity measurement (according to Brookfield's manual, "More solutions to sticky problems"), where N shows the speed of spindle in rpm. Therefore, the suspension's viscosity which does not belong to this range was not measured.

Binder was added to the suspension after 24 hr of initial milling of GDC powder with solvent, dispersant, and plasticizer. As stated in section 4.1-4.3, the aggregates were already formed in initial 24 hr; these aggregates become inter-bridged between the polymeric chains of PVB98. Furthermore, when high τ is applied, the hydrodynamic force does not overcome this bridging of aggregates results in the absence of shear thinning. Due to which the whole suspension is stable and does not show any sedimentation even after five days, which is beneficial during the tape casting, as it does not have any change in microstructure or fluid properties under the application of external τ. Additionally, enhancement of ϕ increases the viscosity, similar to S-I-III.

5. Comparison of Segment-I-IV

From all segments, it can be estimated that the flow behavior dramatically changes with minute changes in the parameters such as ϕ, D, additive content, and additive type. To obtain some vital information about R and ϕ_a in the suspension some numbers have been compared and plotted in Fig. 6(a)-(d), according to Eqs. (12), (13) and (15). First, the values of m and d_f were compared for S-I-III, as shown in Fig. 6(a). As shown in Fig. 2(b), the $[\eta]$ in S-II and III becomes independent of D due to the shear thickening phenomena at high shear rate, so that we did not use it for the calculation of m and d_f in any segment. However, for $\phi > \phi_g$ the yield stress looked promising for the calculation of m and d_f, so Fig. 2(c) and (d) were used for this calculation, according to Eqs. (4) and (10). The values of m and d_f suggest that in all the segments reaction limited cluster aggregation dominates and rigid aggregates formed as shown in Fig. 6(a) [10]. The curves plotted in Fig. 6(b)-(d) correspond to Eqs. (12)-(14), respectively, provide only the tendency of these parameters not the exact numbers. First, the nature of R in different segments was examined by making a logarithmic plot between $\left[1-(\eta_r)^{-\frac{1}{2}}\right]$ and $\left(\frac{\phi}{\phi_m^2}\right)\left(\frac{R}{a}\right)^{3-d_f}$, where the slope of the curve indicates the tendency of R. This whole curve can be split into two zones: the first belongs to diluted area or non-aggregated area and the second one is concentrated or aggregated area. The latter one was considered for evaluation of R. It can be observed from the figure that the slope of the curve is increasing with addition of different polymeric additives. This could be attributed to enhancement of R with addition of polymer. Specifically, addition of long polymeric chains tends to encapsulate a number of primary aggregates along with solvent in it, which increases the slope. These numbers cannot be taken, as it is due to presence of solvent and polymeric chains along with primary aggregates; however, it is indicating the possible hydrodynamic configuration of aggregates

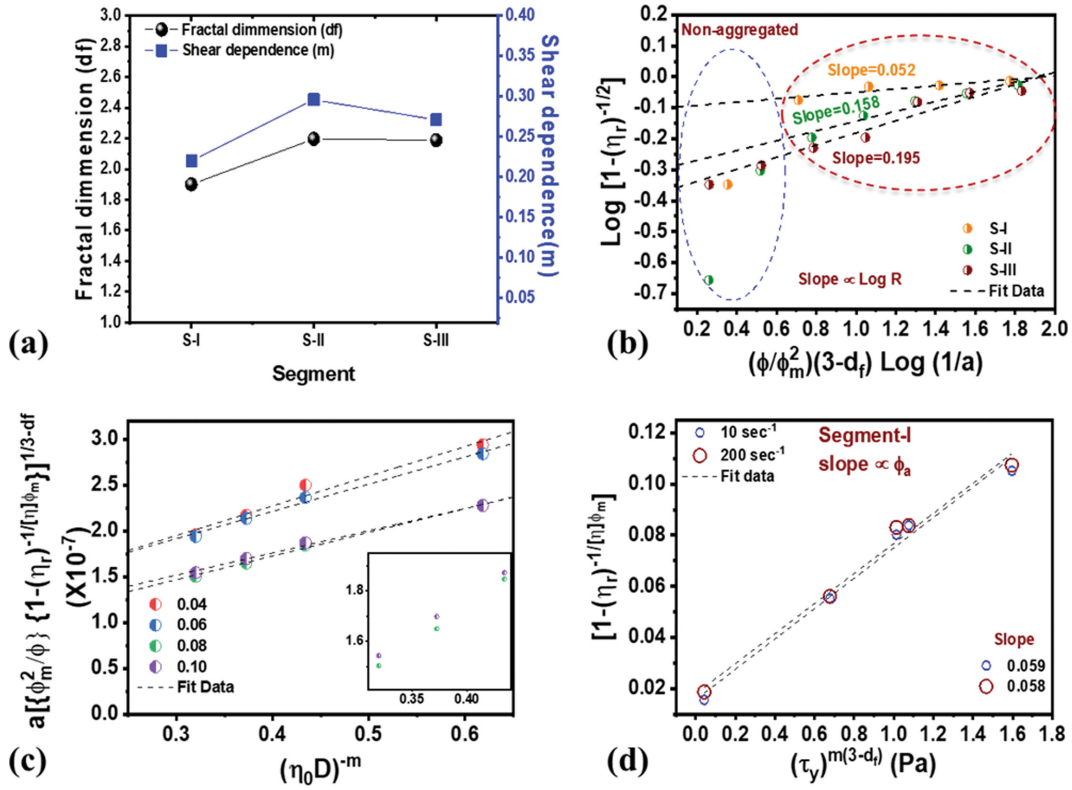

Fig. 6. (a) Comparison of m and d_f values for S-I-III, (b) Log$[1-(\eta_r)^{-1/2}]$ vs ϕ/ϕ_m^2 $(3-d_f)$Log(1/a), (c) a$\left[\left\{\frac{\emptyset_m^2}{\emptyset}\right\}\left\{1-(\eta_r)^{\frac{-1}{[\eta]\phi_m}}\right\}\right]^{\frac{1}{3-d_f}}$ vs $(\eta_0 D)^{-m}$ (d) $[1-(\eta_r)^{-1/[\eta]\phi_m}]$ vs $(\tau_y)^{m(3-d_f)}$.

and polymeric additives. Inspired by these results we further examined the variation of R as function of Ø for Segment-I only, as shown in Fig. 6(c). This curve is plotted according to Eq. (13), where R is proportional to a $\left[\left\{\frac{\emptyset_{m,}^2}{\emptyset}\right\}\left\{1-\eta_r^{\frac{-1}{[\eta]\phi_m}}\right\}\right]^{\frac{1}{3-d_f}}$. As can be observed from the curve, R is decreasing with increasing the particle volume fraction and becomes saturated at Ø=0.08. It can be extracted that the solute particles tends to form new primary aggregates instead of increasing the size of older ones. However after saturation at Ø= 0.08, the particles start to combine with older aggregates and cause microstructural changes (as shown in inset of Fig. 6(c)). Furthermore, Eq. (14) has been used to evaluate the variation of $\emptyset_a$ as function of D as shown in Fig. 6(d). The slope of this curve indicates the tendency of $\emptyset_a$. It can be observed that $\emptyset_a$ was not much affected by D, which implies the rigidness of aggregates. Overall, from Fig. 6 it can be concluded that the aggregates formed are rigid under hydrodynamic conditions and tend to form new aggregates instead of increasing the size of older ones. This interpretation is in good correlation with the obtained m and d_f values (RLCA model). This formation of separated rigid aggregates will help in the formation of crack free green tape during tape casting.

As the present work examines the different factors that can affect the green tape properties at the time of tape casting. Primarily, six parameters affect the compactness, homogeneity, and flexibility of green tape, i.e., ϕ_a, R, D, ϕ_g, d_f, m. As tape casting deals with high particle concentration in the slurry, most of the properties taken into account are related to aggregates instead of particles. In this regime, the gelation point is very crucial to get a crack-free homogeneous tape. The $\phi<\phi_g$ is of no use for tape casting because it leads to slurry flow during shear application and the formation of less compact, cracked green tape. The m value facilitates the prediction of aggregate behavior under application of shear. Higher m value indicates a higher breakage tendency of aggregates during shear application; however, a lower m value indicates a high aggregation tendency, which reduces the homogeneity of the green tape, so the value of m should be close to the m=0.33 [10,32,44,45]. This also implies that the aggregation tendency should be moderate, which could be controlled by addition of dispersant, plasticizer and binders. Beside these suspensions properties, D is the only external property that affect the homogeneity of green tape. Application of excessive τ to the suspension results in the breakage of aggregate into unflocculated secondary particles. This implies that, at the time of casting D should be maintained lower than the value where shear thinning appears. Based on these facts, an optimum composition was found to obtain crack-free, homogeneous green tape shown in Table 2.

Table 2. Composition used for tape preparation

GDC electrolyte substrate		
Ingredient	Volume fraction	Role
GDC10	0.14	Powder
Ethanol	0.365	Solvent
Toluene	0.332	
Fish oil	0.022	Dispersant
BBPS-160	0.01	Plasticizer
PEG8000	0.05	
PVB98	0.08	Binder

6. Surface Morphology of Pre-sintered and Sintered Tape

The composition suggested in Table 2 was found optimum to obtain a crack-free, homogeneous green tape by tape casting. The digital image of crack-free green tape formulated according to the procedure described in section 2.5 is shown in Fig. 7(a) and (b). This tape was pre-sintered at 1,000 °C, 2 hr with an intermediate

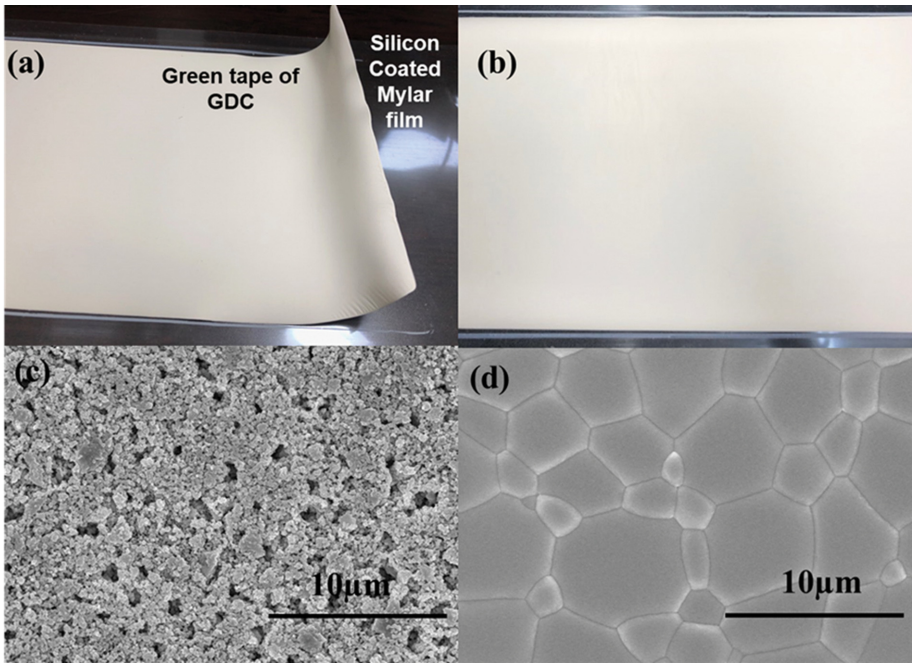

Fig. 7. (a) & (b) Digital image of green tape of GDC after 24 hr of drying at 35 °C, (c) Microstructure of pre sintered Tape and (d) Sintered tape.

step of additive burning at 400 °C for 1 hr. The pre-sintered tape's microstructure was analyzed in terms of scanning electron micrographs, as shown in Fig. 7(c). The microstructure looks pores for this condition due to the burning of polymeric additives and incomplete sintering. To achieve high density tape, the sintering of this tape was conducted at 1,550 °C for 7 hr and the microstructure of the corresponding tape is shown in Fig. 7(d). The high density of tape was achieved by grain growth of GDC particles. The green tape does not have any cracks. The tape is homogeneous, which demonstrates its candidature to support the fabrication of electrolyte supported cells for fuel cell applications.

CONCLUSION

A systematic study was successfully conducted for flow behavior analysis of gadolinium doped ceria based suspension for tape casting. To extract the crucial information about the factors affecting the properties of green tape, different additives were added stepwise and their flow behavior was evaluated. From the application of different scaling relations, it was extracted that, R, ϕ_a, D, ϕ_g, d_f and m are six crucial parameters for tape casting of suspension. The mutual balance between them can provide a crack-free and homogeneous tape, which could be achieved by adjusting the amount of different additives as suggested. These additives' adjustment causes their surficial reactions with GDC powder in hydrodynamic conditions, which induce extensive changes in the flow behavior of suspension and extension of ϕ_g, which is a crucial parameter to get an applicable tape. The enhancement of R and ϕ_a in the presence of different additives beyond ϕ_g, suggests facilitation of aggregation and extension of the limit of ϕ in these cases. This extension is very useful to get high yield of final tape with minimum additive addition.

ACKNOWLEDGEMENTS

This work was supported by the Korea Institute of Energy Technology Evaluation and Planning (KETEP) and the Ministry of Trade, Industry & Energy (MOTIE) of the Republic of Korea (No. 20213030040110) and National Research Foundation of Korea (NRF) grant funded by the Korea government (MSIT) (2018R1 A5A 1025224).

DECLARATION OF INTEREST

There is no conflict of interest.

SUPPORTING INFORMATION

Additional information as noted in the text. This information is available via the Internet at http://www.springer.com/chemistry/journal/11814.

REFERENCES

1. U. Hennings and R. Reimert, *Appl. Catal. B Environ*., **70**, 498 (2007).
2. C. Y. Chen and C. L. Liu, *Ceram. Int.*, **37**, 2353 (2011).
3. A. Arabac and M. F. Öksüzömer, *Ceram. Int.*, **38**, 6509 (2012).
4. L. He, Y. Su, J. Lanhong and S. Shi, *J. Rare Earths*, **33**, 791 (2015).
5. C. Son, A. Bhardwaj, J. Hong, J. W. Kim, H. S. Moon, H. S. Noh and S. J. Song, *J. Ceram. Process. Res.*, **18**, 858 (2017).
6. A. Nazir, H. T. T. Le, C. W. Min, A. Kasbe, J. Kim, C. S. Jin and C. J. Park, *Nanoscale*, **12**, 1629 (2020).
7. L. Mathur, I. H. Kim, A. Bhardwaj, B. Singh, J. Y. Park and S. J. Song, *Compos. Part B Eng*., **202**, 108405 (2020).
8. L. Mathur, A. Kumar, I. H. Kim, H. Bae, J. Y. Park and S. J. Song, *J. Power Sources*, **493**, 229696 (2021).
9. M. N. Rahaman, *Ceramic processing and sintering*, CRC Press, Boca Raton (2003).
10. H. Lee and S. Koo, *Korea Aust. Rheol. J.*, **28**, 267 (2016).
11. D. Kim and S. Koo, *Korea Aust. Rheol. J.*, **30**, 67 (2018).
12. K. Lindqvist and E. Lidén, *J. Eur. Ceram. Soc.*, **17**, 359 (1997).
13. S. F. Corbin and P. S. Apté, *J. Am. Ceram. Soc.*, **82**, 1693 (1999).
14. A. Sarikaya and F. Dogan, *Ceram. Int.*, **39**, 403 (2013).
15. H. Moon, S. D. Kim, S. H. Hyun and H. S. Kim, *Int. J. Hydrogen Energy*, **33**, 1758 (2008).
16. S. Ramanathan, K. P. Krishnakumar, P. K. De and S. Banerjee, *J. Mater. Sci*., **39**, 3339 (2004).
17. J. Seol, M. Young, E. Jeong, J. Moon and H. Jin, *Solid State Ionics*, **42**, 4546 (2016).
18. C. Grings Schmidt, K. K. Hansen, K. B. Andersen, Z. Fu, A. Roosen and A. Kaiser, *J. Eur. Ceram. Soc*., **36**, 645 (2016).
19. L. Ren, P.-Y. Zeng and J. Dongliang, *J. Am. Ceram. Soc.*, **90**, 3001 (2007).
20. L. Ren, Y. P. Zeng, and D. Jiang, *Solid State Sci*., **12**, 138 (2010).
21. N. Das and H. S. Maiti, *J. Membr. Sci*., **140**, 205 (1998).
22. N. Das, S. Bandyopadhyay, D. Chattopadhyay and H. S. Maiti, *J. Mater. Sci*., **31**, 5221 (1996).
23. N. Das and H. S. Maiti, *J. Phys. Chem. Solids*, **70**, 1395 (2009).
24. D. Hotza and P. Greil, *Mater. Sci. Eng. A*, **202**, 206 (1995).
25. G. J. Fleer and J. Lyklema, *J. Colloid Interface Sci*., **46**, 1 (1974).
26. J. X. Zhang, D. L. Jiang, S. H. Tan, L. H. Gui and M. L. Ruan, *J. Mater. Res*., **17**, 2019 (2002).
27. J. Wang and L. Gao, *Ceram. Int.*, **26**, 187 (2000).
28. L. H. Luo, A. I. Y. Tok and F. Y. C. Boey, *Rengong Jingti Xuebao/Journal Synth. Cryst*., **37**, 188 (2006).
29. T. Chartier and A. Bruneau, *J. Eur. Ceram. Soc*., **12**, 243 (1993).
30. L. P. Meier, L. Urech and L. J. Gauckler, *J. Eur. Ceram. Soc*., **24**, 3753 (2004).
31. B. Lee and S. Koo, *Powder Technol*., **266**, 16 (2014).
32. J. Cho and S. Koo, *J. Ind. Eng. Chem*., **27**, 218 (2015).
33. J. Hong, C. Balamurugan, H.-N. Im, S.-Y. Jeon, Y.-S. Yoo and S.-J. Song, *J. Electrochem. Soc*., **165**, F132 (2018).
34. I. M. Krieger and T. J. Dougherty, *Trans. Soc. Rheol*., **3**, 137 (1959).
35. N. Casson, *Rheology of disperse systems*, New York, NY (1959).
36. T. L. Smith and C. A. Bruce, *J. Colloid Interface Sci*., **72**, 13 (1979).
37. A. A. Potanin, *J. Colloid Interface Sci*., **157**, 399 (1993).
38. D. Quemada, *Rheol. Acta*, **16**, 82 (1977).
39. N. Willenbacher and K. Georgieva, *Prod. Des. Eng. Formul. Gels Pastes*, 1 (2013).
40. F. J. Galindo-Rosales, F. J. Rubio-Hernández and J. F. Velázquez-Navarro, *Rheol. Acta*, **48**, 699 (2009).
41. S. R. Raghavan and S. A. Khan, *J. Colloid Interface Sci*., **185**, 57

(1997).
42. G. O. Medowski and R. D. Sutch, *Doctor Blade Process in F.F.Y.*, 9th ed., Ceramic fabrication processes, Acadamic Press, New York, NY (1976).
43. C. W. Nies and G. L. Messing, *J. Am. Ceram. Soc.*, **67**, 301 (1984).
44. J. Jeon and S. Koo, *J. Magn. Magn. Mater.*, **324**, 424 (2012).
45. S. Koo, *J. Ind. Eng. Chem.*, **14**, 679 (2008).

Supporting Information

Flow behavior of gadolinium doped ceria under different polymeric and hydrodynamic environment for tape casting application

Lakshya Mathur*, Hohan Bae*, Yeon Namgung*, Jun-Young Park,†, and Sun-Ju Song*,†**

*Department of Materials Science and Engineering, Chonnam National University, Gwangju 61186, Korea
**HMC, Department of Nanotechnology and Advanced Materials Engineering, Sejong University, Seoul 05006, Korea
(*Received 10 May 2022 • Revised 25 July 2022 • Accepted 21 August 2022*)

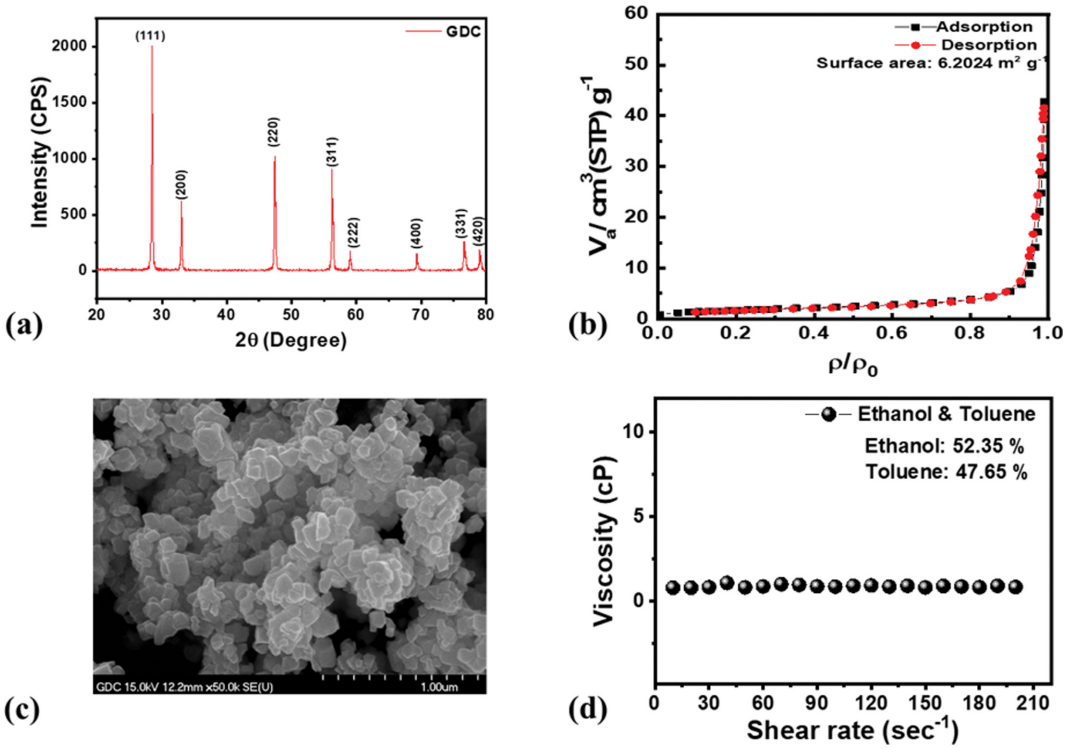

Fig. S1. (a) XRD of commercial GDC powder, (b) Adsorption desorption isotherm for GDC powder under N_2 atmosphere preheated at 150 °C, 6 h, (c) Microstructure of commercial GDC powder, (d) Viscosity as function of shear rate for suspending medium (mixture of ethanol and toluene).